Periodic orbits in Hamiltonian chaos of the annular billiard

G. Gouesbet, S. Meunier-Guttin-Cluzel, and G. Grehan
Laboratoire d'Energétique des Systèmes et Procédés (LESP), Institut National des Sciences Appliquées de Rouen et Université de Rouen, Unité Mixte de Recherche (UMR) 6614, du Centre National de la Recherche Scientifique (CNRS), CORIA (Complexe de Recherche Interprofessionnel en Aérothermochimie), Boîte Postale 08, 76131 Mont Saint Aignan Cedex, France
(Received 20 April 2001; published 18 December 2001)

We consider the motion of trajectories in the annular billiard, constituted of a circle with an internal, perfectly reflecting, eccentrically located secondary circle, displaying a generic Hamiltonian behavior (including periodic orbits, invariant curves, and chaotic areas). Periodic orbits embedded in the phase space are systematically investigated, with a focus on inclusion-touching periodic orbits, up to symmetrical orbits of period 6. Candidates for periodic orbits are detected by investigating grayscale distance charts and, afterward, each candidate is validated (or rejected) by using analytical and/or numerical methods. This Hamiltonian problem with Hamiltonian chaos (mechanical language) may equivalently be viewed as an optical problem with optical chaos (expressed with a geometrical optics language). It then may be extended to the study of interaction between a laser beam (or a plane wave as a limit) and a sphere with an eccentrically located spherical inclusion, this interaction being described by a generalized Lorenz-Mie theory recently established. Inclusion-touching periodic orbits in the annular billiard may generate a new class of morphology-dependent resonances in the associated extended generalized Lorenz-Mie theory problem.

DOI: 10.1103/PhysRevE.65.016212 PACS number(s): 05.45.−a

I. INTRODUCTION

Let us consider the interaction between an electromagnetic wave and a perfect homogeneous sphere and focus our attention on internal fields. Morphology-dependent resonances (MDRs), also called whispering gallery modes (WGMs), correspond to solutions of characteristic equations associated with boundary conditions, and occur at resonance frequencies that are poles of field coefficients [1,2]. At resonance frequencies, MDRs generate intense internal fields which are concentrated near the rim of the scatterer and may activate a host of nonlinear effects, including lasing [3]. In a geometrical optics (ray tracing) picture, MDRs are associated with rays that undergo multiple reflections inside the scatterer and without any refractive escape, upon resonance, satisfy a phase-matching condition, corresponding to enhanced field intensities. Equivalently, we may view an equatorial plane of the sphere as a mechanical billiard, defining a Hamiltonian mechanical problem. MDRs are then associated with a class of periodic orbits (without refractive escape, see complementary discussion in Sec. III H) of the Hamiltonian problem expressed in terms of trajectories. This so-defined circular billiard is integrable in the mechanical sense [4,5] and, therefore, only exhibits periodic orbits, and invariant curves in a phase space description (no chaotic area).

The characteristic equations allowing one to predict resonance frequencies do not depend on the illuminating beam. This does not mean, however, that the structure of the illuminating beam is irrelevant. Indeed, MDRs have to be excited from outside, and, therefore, the coupling between the illuminating beam and the internal field is a key issue [6,7]. The study of such a coupling may be achieved in the framework of generalized Lorenz-Mie theories (GLMTs) that describe the interaction between an arbitrary shaped beam (continuous or pulsed) and some regular particles [8,9]. These regular particles must be such that Maxwell's equations can be solved by relying on a method of separation of variables. We then say that we are facing an exactly solvable electromagnetic problem. An example of applications of a GLMT to MDRs is available from Ref. [10].

Laser beam scattering by a sphere is an exactly solvable problem, leading to what is called the GLMT in the strict sense (Ref. [11] and references therein). As aforementioned, the associated Hamiltonian billiard problem is integrable. Recently, a GLMT for a sphere with an eccentrically located spherical inclusion, with the inclusion being dielectric or perfectly reflecting, has been established [12]. Similarly, along the same lines, a GLMT for a circular cylinder, with an eccentrically located circular cylinder as an inclusion, should be technically feasible [8]. In both cases, a restricted associated Hamiltonian problem, with the inclusion being perfectly reflecting, leads to the annular billiard. This billiard deals with trajectories in an annular space bounded by a host (external) circle, and an internal, perfectly reflecting, eccentrically located secondary circle. In contrast with the circular billiard, the Hamiltonian annular billiard is not integrable, and leads to generic [5] Hamiltonian behavior, including chaotic motion [13–16]. Therefore, we are facing the situation of a billiard that is nonintegrable while its extended electromagnetic counterpart is exactly solvable.

Hamiltonian chaos in the mechanical language is called optical chaos in the geometrical optics language, and has been studied in the case of asymmetric resonant cavities (ARCs) [17,18] with interesting applications concerning Q spoiling in deformed ring cavities and the behavior of lasing droplets [19,20]. However, the electromagnetic problem associated with ARCs is not exactly solvable.

A study of the annular billiard (with the extended electromagnetic problem in mind) is then of particular interest because this system simultaneously shares the properties of nonintegrability and exact solvability. In particular, periodic orbits are expected to provide specific signatures in electro-

magnetic scattering features. In the case of three-dimensional (3D) strongly dissipative systems, with chaotic attractors, periodic orbits are all unstable, densely embedded, and provide a skeleton of the attractor that may be characterized by a template and a population of periodic orbits, leading to a topological characterization (Refs. [21–23] and references therein). Any trajectory in the chaotic attractor has a recurrent behavior and shadows any periodic orbit, during finite intervals of time. The determination of the periodic solutions then happens to be equivalent to the knowledge of all solutions.

Similarly, the knowledge of periodic solutions is of utmost importance for a Hamiltonian system. However, in contrast with dissipative systems, periodic solutions do not, in general, shadow aperiodic ones because Hamiltonian systems do not possess any attractor, and chaotic solutions are area filling (when the system can be reduced to two coordinates, as in the annular billiard), or volume (hypervolume) filling. Furthermore, periodic solutions may be stable, unstable, or neutral [4,5]. Periodic solutions are nevertheless of interest because they structure, at least locally, the phase space [4]. Also, for billiards, they receive an optical interpretation with significant consequences on scattering features in the extended electromagnetic problem, such as concerning MDRs for the circular billiard.

The aim of this paper is, therefore, to study periodic orbits in the annular billiard. This billiard is chosen because (i) it simultaneously shares the properties of nonintegrability and electromagnetic exact solvability and, (ii) with the associated GLMT, it opens the way to the optical characterization of a class of nonhomogeneous particles. Furthermore, because the status of periodic orbits in a billiard is different than the one for 3D strongly dissipative systems, specific tools have to be developed.

The paper is organized as follows. Section II presents the annular billiard, its generic Hamiltonian behavior, and derives a number of equations to be used later, for the validation (or rejection) of candidates for periodic orbits. Section III presents the grayscale distance charts allowing one to detect candidates, the analytical-numerical techniques to be used to validate (or reject) the candidates, and a commented catalog of the periodic orbits up to $(N=6)$-symmetrical orbits. Some further comments and prospective sections are also provided. Section IV presents our conclusion. Technicalities concerning the validation of periodic orbits in the catalog are reported in the Appendix.

II. THE ANNULAR BILLIARD AND ITS EQUATIONS

A. The annular billiard

We consider a circular boundary B, with a radius R set equal to 1, without any loss of generality. Inside this boundary, we insert a secondary circle (called the inclusion in reference to the extended GLMT electromagnetic problem), with a radius $r<1$, eccentrically located, defined by its boundary B' (Fig. 1). The center of the host circle is located at the origin O of a Cartesian coordinate system (xOy). The center O' of the inclusion is located on the axis Oy (again without any loss of generality). The location of O' with respect to O is algebraically defined as $y(O')=d$. We limit our investigation to the case $d>0$. The case $d=0$ is of limited interest because the Hamiltonian system is then integrable. The case $d<0$ is equivalent to the case $d>0$ through a π rotation of the figure. This configuration is traditional in the electromagnetic context [12] but differs from the one in Refs. [13–14] in which the center O' is located on the axis Ox. In the billiard, trajectories are straight lines excepted at impacts (on the host circle and on the inclusion) with the Snell-Descartes law being satisfied (the angle of reflection is equal to the angle of incidence).

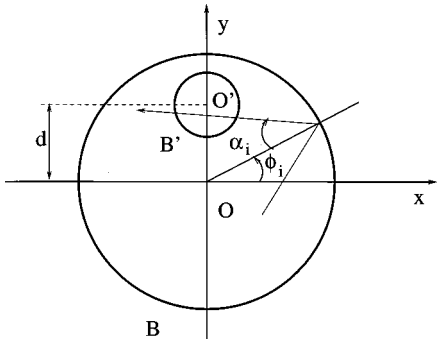

FIG. 1. The annular billiard.

B. Phase space

The annular billiard exhibits two degrees of freedom and, therefore, requires a four-dimensional phase space. Due to the conservation of energy, the motion takes place on a three-dimensional hypersurface and its description can, therefore, be reduced to a two-dimensional mapping, by using a Poincaré surface of section. The two variables for the mapping are chosen to be two stroboscopic angles (φ, α) characterizing an impact of the trajectory on the host circle. The space (φ, α) is then a reduced phase space [4] and is simply called the phase space in this paper.

Angles and conventions are displayed in Fig. 2. The angle

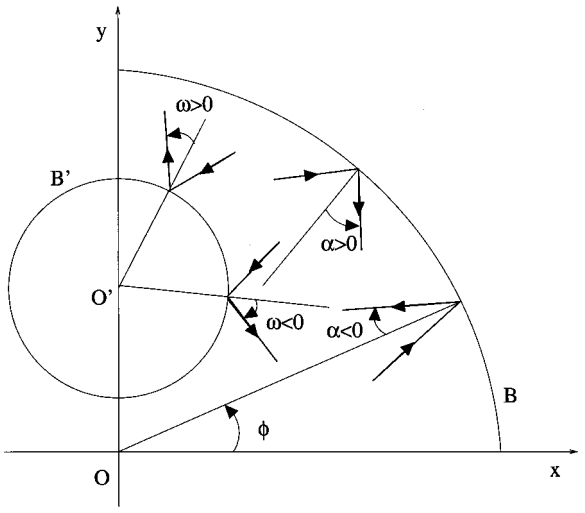

FIG. 2. Angles and conventions for angles in the annular billiard.

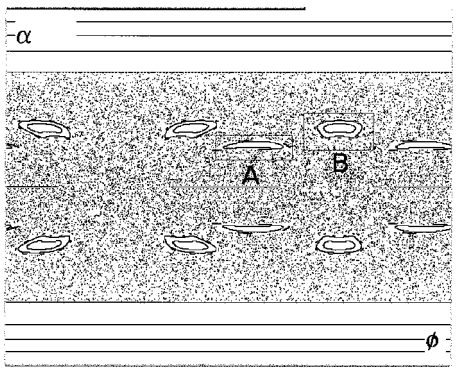

FIG. 3. Genericity of the annular billiard.

$\varphi \in [0,2\pi]$ defines the location of an impact on B. It is measured from axis x, in the usual counterclockwise fashion. With $R=1$, the measure φ of the location is equivalent to the measure $s=\varphi$ of an arc length on the host circle. The angle $\alpha \in [-\pi/2,+\pi/2]$ defines the direction of propagation after impact, measured from the normal to the host circle. The modulus of the tangential momentum at impact is then $p=\sin\alpha$, positive or zero when $\alpha \in [0,2\pi]$, i.e., when the vectorial component of the tangential momentum is oriented counterclockwise, and negative otherwise. Impacts on the inclusion are characterized by an angle ω, as defined in Fig. 2. The angle ω is not a phase space coordinate since the phase space is 2D, but will be convenient for algebraic manipulations. The nonintegrability of the system arises from the fact that the tangential momentum is not preserved when the trajectory hits the inclusion between two impacts on the host circle.

C. Genericity of the annular billiard

The parameters d (location of the inclusion) and r (radius of the inclusion) are control parameters of the system. In this paper, explicit calculations are carried out for $d=0$, 5, $r=0$, 35. The genericity [5] of the annular billiard for these control parameter values is illustrated in Fig. 3 displaying a sample of trajectories starting from different initial conditions in the (φ, α) phase space (such a representation is here called a Hamiltonian chart).

For $|\alpha|$ large enough, we may observe fixed points corresponding to inclusion non-touching periodic orbits. These are the MDRs, with rational winding numbers, of the circular billiard. Still for $|\alpha|$ large enough, we observe invariant Kolmogorov-Arnold-Moser (KAM) curves, with $\alpha=$const, i.e., $p=$const, which are the invariant KAM curves of the circular billiard, with irrational winding numbers. For smaller values of $|\alpha|$, we are dealing with inclusion-touching trajectories. The Hamiltonian chart then exhibits two dominant stable periodic orbits (as we shall see later these are $N=4$ and $N=6$ periodic orbits) surrounded by islands (invariant KAM curves associated with the stability of these orbits), immersed in an area-filling chaotic sea.

D. Mappings and area-preservation

Let us consider a piece of trajectory from initial impact (φ_0,α_0) to next impact (φ_1,α_1). We must then distinguish two mappings:

(i) $M_0:(\varphi_0,\alpha_0)\rightarrow(\varphi_1,\alpha_1)$ if the piece does not hit the inclusion.

(ii) $M_1:(\varphi_0,\alpha_0)\rightarrow(\varphi_1,\alpha_1)$ if the piece does hit the inclusion.

From geometric considerations, we establish the hitting condition for the mapping M_1,

$$r \geqslant |d\cos(\varphi_0+\alpha_0)+\sin\alpha_0|, \tag{1}$$

in which the sign ''equal'' is for grazing incidence on the inclusion. We have an obvious complementary condition for the mapping M_0.

The M_0 mapping is established to read as

$$\varphi_1=\varphi_0+2\alpha_0+\varepsilon\pi, \tag{2}$$

$$\alpha_1=\alpha_0, \tag{3}$$

in which $\varepsilon=+1$ for a piece running counterclockwise without crossing the semi-axis Ox, and $\varepsilon=-1$ for a piece running clockwise without crossing the semi-axis Ox. It is actually convenient to set $\varepsilon=+1$ as in Ref. [14]. Then, φ is to be understood modulo 2π. Recall, however, than $\varphi \in [0,2\pi]$. Then, in Eq. (2) and, similarly, in other equations to come, we have to carefully evaluate the exact modulo determination to be chosen. In practice, these equations will be used to validate periodic orbits already detected. Therefore, the most expedient and efficient way to choose the proper modulo determination is to check on a drawing of the periodic orbit under study.

For the M_1 mapping, we obtain (after more effort)

$$\sin\omega_0=\frac{-1}{r}[\sin\alpha_0+d\cos(\varphi_0+\alpha_0)], \tag{4}$$

$$\varphi_1-\alpha_1=\varphi_0+\alpha_0+2\omega_0, \tag{5}$$

$$\sin\alpha_1=-r\sin\omega_0+d\cos(\varphi_1-\alpha_1), \tag{6}$$

in which the angle of reflection ω on the inclusion (not a phase-space coordinate) is conveniently introduced. Equations (1)–(6) agree with the ones given in Ref. [14] under a change of convention $\varphi=\theta-\pi/2$, $\alpha\rightarrow-\alpha$.

M_0 mapping is readily checked to be area preserving, both with coordinates (φ, α) and $(s,p)=(\varphi,\sin\alpha)$. It is also a fact, but more tricky to check, that the M_1 mapping is area-preserving in terms of coordinates (s, p), but not in terms of (φ, α), in agreement with a remark by Berry [5]. Since any mapping $M_{(n)}:(\varphi_0,\alpha_0)\rightarrow(\varphi_n,\alpha_n)$ is a product of M_0 and M_1 mappings, it then follows that the annular billiard is Hamiltonian (area preserving) in terms of coordinates (s, p).

E. Mapping sequences

A piece of trajectory with n impacts including the initial impact (φ_0,α_0), i.e., with $(n-1)$ elementary pieces, is characterized by a mapping $M_{(n-1)}$ which is a product of $(n-1)$ submappings M_0 and M_1 according to

$$M_{(n-1)}=M_{i_{n-1}}M_{i_{n-2}}\ldots M_{i_1}, \tag{7}$$

in which i_j's ($j=1\ldots n-1$) are 0's or 1's and, by convention, the rightmost submapping $M_{i_1}:(\varphi_0,\alpha_0)\rightarrow(\varphi_1,\alpha_1)$ is the first submapping encountered along the piece of trajectory. Conveniently dropping the uppercase letters M, the piece of trajectory is then characterized by a sequence of 0's and 1's, denoted S_P and called the mapping sequence of the piece of trajectory P,

$$S_P=i_{n-1}i_{n-2}\ldots i_1. \tag{8}$$

F. Periodic orbits, equivalence classes, and admissible mapping sequences

By definition, a periodic orbit of period N (we have $N\geqslant 1$) satisfies

$$(\varphi_{n+N},\ \alpha_{n+N})=(\varphi_n,\ \alpha_n), \tag{9}$$

and possesses a mapping that is a product of N submappings M_0 and M_1, with coordinate endpoints identified. We also assume that we only consider prime periodic orbits, i.e., N is not a multiple of another integer $N'<N$ that would also satisfy Eq. (9). The geometrical figure depicting a periodic orbit is invariant under:

(i) a change of the initial impact (φ_n,α_n), which is equivalent to a time translational invariance, and to a Bernoulli shift on the mapping sequence.

(ii) A change of the sign of the initial angle α_n, which is equivalent to a time reversal invariance and to a reversal of the mapping sequence.

These invariances are well exemplified in the Hamiltonian chart for two classes of orbits, later discussed [4 (2) 1 and 6 (2) 1 in the catalog of Sec. III B].

We, therefore, define equivalence classes of periodic orbits in which all periodic orbits displaying the same geometrical picture are equivalent. This implies that all periodic orbits in an equivalence class possess the same mapping sequences modulo reversals and shifts of mapping sequences. Mind however that equivalent mapping sequences may be shared by periodic orbits pertaining to different classes [such as the ones associated with 6 (4) 1 and 6 (4) 2 in the catalog].

Periodic orbits may be inclusion touching or non-inclusion-touching. The set of non-inclusion-touching periodic orbits contains all MDRs (WGMs) of the circular billiard (relevant to light scattering by spheres), with mapping sequences having the form $\ldots 000\ldots$, i.e., exhibiting only the symbol 0. Their discussion is classical (and trivial) in the Hamiltonian framework and is omitted from this paper [17].

Inclusion-touching periodic orbits (from now on, simply called periodic orbits when there is no ambiguity), conversely possess mapping sequences containing at least one symbol 1. We shall provide a catalog of equivalence classes of periodic orbits, in which each class is displayed via one representative, with the following conventional condition: the mapping sequence of the representative must maximize the number of 1's on its right most locations. Such a mapping sequence is called an admissible mapping sequence. Let us note that this condition does not always uniquely determine the representative [more than one representative in the same class may share the same admissible mapping sequence, see examples in the catalog of Sec. III B, such as for the class of 2 (1) 1 that possesses two admissible representatives]. From now on, initial conditions denoted as (φ_0,α_0) are reserved for admissible representatives, i.e., having admissible mapping sequences.

TABLE I. Admissible mapping sequence for periodic orbits up to period $N=6$

Sequences	Label	Occurrence
1	1 (1)	2*S*
01	2 (1)	1*S*,1*NS*
11	2 (2)	none
001	3 (1)	none
011	3 (2)	1*S*,1*NS*
111	3 (3)	none
0001	4 (1)	1*S*
0101	4 (2)	1*S*
0011	4 (3)	none
0111	4 (4)	1*S*,1*NS*
1111	4 (5)	none
00001	5 (1)	1*S*,1*NS*
00101	5 (2)	none
00011	5 (3)	2*S*,1*NS*
01011	5 (4)	1*S*,2*NS*
00111	5 (5)	1*S*,1*NS*
01111	5 (6)	2*S*,1*NS*
11111	5 (7)	none
000001	6 (1)	1*S*
001001	6 (2)	1*S*
000101	6 (3)	1*S*
000011	6 (4)	2*S*
010101	6 (5)	1*S*
001011	6 (6)	none
000111	6 (7)	2*S*
011011	6 (8)	4*S*
010111	6 (9)	1*S*
001111	6 (10)	2*S*
011111	6 (11)	1*S*
111111	6 (12)	none

The Hamiltonian chart of Fig. 3 exhibits a visually dominant period-six stable periodic orbit that is symmetrical (as we shall see, there are symmetrical and nonsymmetrical periodic orbits). Therefore, the catalog of representatives will be drawn up to $N=5$ for symmetrical and nonsymmetrical periodic orbits and up to $N=6$ for symmetrical orbits. Accordingly, Table I lists all admissible mapping sequences up to $N=6$ in the first column.

Column 2 in Table I designates the admissible mapping sequences by a label $A(B)$ that will be later used to label the representatives displayed in the catalog, in which $A=N$ is the period of the sequence (orbit) and B is an ordinal positive integer allowing one to order the admissible mapping sequences for a given N. The period N being fixed, let us con-

sider two admissible mapping sequences S_1 and S_2 with labels $N(B_1)$ and $N(B_2)$, respectively. We say that S_1 is smaller than $S_2 (S_1 < S_2)$ iff $B_1 < B_2$ according to the integer natural order. For instance, $01 < 11$. The rules used to define the admissible mapping sequence order are as follows. Let M be the number of 1's in a sequence. Let us consider two sequences S_1 and S_2 sharing the same period N and two different values of M, M_1 and M_2, respectively. If $M_1 < M_2$, then $S_1 < S_2$. Next, let us consider two sequences S_1 and S_2 sharing the same period N and the same value of M. Then $S_2 > S_1$ iff the number of symbols 1 larger in S_2 than in S_1, in the rightmost parts of the sequences.

Now, let us consider an admissible mapping sequence S with period N and M symbols 1. Let us map S to a conjugate S^* by changing 0's to 1's and 1's to 0's. We obtain the mapping sequence of a periodic orbit but this sequence is not necessarily admissible and the periodic orbit is, therefore, not necessarily an admissible representative of the equivalence class. For instance, $S = 00101$ is mapped to $S^* = 11010$, which is not admissible (the associated admissible mapping sequence is 01011). Similarly, the time reversal invariance ($\alpha \leftrightarrow -\alpha$) concerns equivalence classes but not necessarily admissible representatives. For instance, under time reversal, the admissible mapping sequence $S = 0011$ is mapped to $S' = 1100$, which is not admissible. In the catalog of representatives, it will then be necessary to specify an initial condition φ_0 and an arrow of time (sign of α_0) ensuring that the displayed periodic orbit is an admissible representative of its equivalence class. The symmetry of the Hamiltonian chart of Fig. 3 with respect to $\alpha = 0$ is then associated with the fact that this chart displays all elements of an equivalence class, including nonadmissible periodic orbits.

Finally, because an admissible mapping sequence does not necessarily generate any periodic orbit, Table I displays a third column (occurrence) to be later commented when the catalog is presented.

G. Basic equations

We call ''basic equations'' the equations, for periodic orbits, which concatenate submappings M_0 and M_1 equations for a given mapping sequence. In this paper, we shall only deal with basic equations for admissible mapping sequences [see the example of Eqs. (10)–(19) in the next section]. In principle, basic equations then allow one to determine all periodic orbits associated with a given admissible mapping sequence. In practice, solving a set of basic equations is impossible, excepted for simple special cases (small values of the period N). Basic equations are then better used to validate (or reject) candidates of period orbits detected in a previous step (Sec. III).

H. Derived equations for admissible mapping sequences 0 . . . 01 . . . 1

An admissible representative is determined by two initial values φ_0 and α_0, therefore, requiring two equations (expected for special cases, when a single equation, say for α_0, can be established, with examples in the Appendix). Such two equations may be obtained from the set of basic equations, and are called derived equations. In this section, we establish derived equations for admissible mapping sequences of the form $0 \ldots 01 \ldots 1$, with M symbols 1, followed by $(N\text{-}M)$ symbols 0 (we recall that mapping sequences are read from right to left). All admissible mapping sequences are of this form up to $N = 3$ included (Table I).

B asic equations read as

$$\sin \omega_j = \frac{1}{r}[-\sin \alpha_j - d \cos(\varphi_j + \alpha_j)], \quad j = 0 \ldots M-2, \tag{10}$$

$$\varphi_{j+1} - \alpha_{j+1} = 2\omega_j + \varphi_j + \alpha_j . \tag{11}$$

$$\sin \alpha_{j+1} = -r \sin \omega_j + d \cos(\varphi_{j+1} - \alpha_{j+1}), \tag{12}$$

$$\sin \omega_{M-1} = \frac{1}{r}[-\sin \alpha_{M-1} - d \cos(\varphi_{M-1} + \alpha_{M-1})], \tag{13}$$

$$\varphi_M - \alpha_M = 2\omega_{M-1} + \varphi_{M-1} + \alpha_{M-1}, \tag{14}$$

$$\sin \alpha_M = -r \sin \omega_{M-1} + d \cos(\varphi_M - \alpha_M), \tag{15}$$

$$\varphi_j = \varphi_{j-1} + 2\alpha_{j-1} + \pi, j = M+1 \ldots N-1, \tag{16}$$

$$\alpha_j = \alpha_{j-1}, \tag{17}$$

$$\varphi_0 = \varphi_{N-1} + 2\alpha_{N-1} + \pi, \tag{18}$$

$$\alpha_0 = \alpha_{N-1}, \tag{19}$$

in which we conveniently dropped the symbol ϵ in Eqs. (16) and (18), see Eq. (2), with φ being understood modulo 2π (for applications, recall, however, that $\varphi \in [0, 2\pi]$). Also, we isolated the Mth mapping M_1 in Eqs. (13)–(15) for later convenience.

Using iteratively Eq. (10) for $j = 0$, Eq. (12) for $j = 0$, Eq. (10) for $j = 1$, Eq. (12) for $j = 1, \ldots$, ending with Eqs. (13), (15), and using Eqs. (17), (19), we establish

$$\cos(\varphi_0 + \alpha_0) = -\cos(\varphi_M - \alpha_0) - \sum_{i=1}^{M-1} [\cos(\varphi_i + \alpha_i) + \cos(\varphi_i - \alpha_i)]. \tag{20}$$

Next, from Eqs. (16)–(19)

$$\varphi_M = \varphi_0 - (N-M)(\pi + 2\alpha_0). \tag{21}$$

Using Eq. (11) and a recurrence technique

$$\varphi_i - \alpha_i = \varphi_0 + \alpha_0 + 2\left[\sum_{j=0}^{i-1} \omega_j + \sum_{j=1}^{i-1} \alpha_j\right], \quad i = 1 \ldots M-1, \tag{22}$$

from which we also have

$$\varphi_i + \alpha_i = \varphi_0 + \alpha_0 + 2\left[\sum_{j=0}^{i-1} \omega_j + \sum_{j=1}^{i} \alpha_j\right], \quad i = 1 \ldots M-1. \tag{23}$$

Equation (20) then becomes

$$\cos(\varphi_0 + \alpha_0) + \cos[\varphi_0 - \alpha_0 - (N-M)(\pi + 2\alpha_0)] + \sum_{i=1}^{M-1} \left\{ \cos\left[\varphi_0 + \alpha_0 + 2\left(\sum_{j=0}^{i-1} \omega_j + \sum_{j=1}^{i-1} \alpha_j\right)\right] + \cos\left[\varphi_0 + \alpha_0 + 2\left(\sum_{j=0}^{i-1} \omega_j + \sum_{j=1}^{i} \alpha_j\right)\right]\right\} = 0, \tag{24}$$

to be complemented by the following readily established equations (use a recurrence technique), for $j = 0 \ldots M-2$

$$\omega_j = \arcsin\left\{\frac{1}{r}\left[-\sin\alpha_j - d\cos\left(\varphi_0 + \alpha_0 + 2\sum_{i=0}^{j-1} \omega_i + 2\sum_{i=1}^{j} \alpha_i\right)\right]\right\}, \tag{25}$$

$$\alpha_{j+1} = \arcsin\left\{-r\sin\omega_j + d\cos\left(\varphi_0 + \alpha_0 + 2\sum_{i=0}^{j} \omega_i + 2\sum_{i=1}^{j} \alpha_i\right)\right\}. \tag{26}$$

In deriving Eq. (20), we had to divide by d, therefore, dismissing the case $d = 0$ (integrable system). In the sequel, this equation will be conveniently called the first equation (FE) for the mapping sequence under study.

For the second equation (SE), we invoke Eq. (14), which has not yet been used, and establish

$$\omega_{M-1} + \alpha_0 + (N-M)\left(\frac{\pi}{2} + \alpha_0\right) + \sum_{j=0}^{M-2} \omega_j + \sum_{j=1}^{M-1} \alpha_j = 0, \tag{27}$$

which (with φ understood as being modulo 2π) is to be understood modulo π. This SE is to be complemented by

$$r\sin\omega_{M-1} = -\sin\alpha_{M-1} - d\cos\left(\varphi_0 + \alpha_0 + 2\sum_{j=0}^{M-2} \omega_j + 2\sum_{j=1}^{M-1} \alpha_j\right) = -\sin\alpha_0 + d\cos[\varphi_0 - \alpha_0 - (N-M)(\pi + 2\alpha_0)]. \tag{28}$$

In Eq. (28), we have two variants to evaluate ω_{M-1}. The best variant to be chosen, before insertion into Eq. (27), may depend on the mapping sequence under study.

I. Derived equations for arbitrary admissible mapping sequences

Mapping sequences of the form $0 \ldots 01 \ldots 1$, previously considered, may be symbolically denoted as $P_1 M_1$, in which $M_1 = M$ designates the number of symbols 1 and $P_1 = (N - M)$ designates the number of symbols 0. Arbitrary admissible mapping sequences may then be symbolically denoted as $P_K M_K \ldots P_2 M_2 P_1 M_1$, in a similar way. For further use, we introduce the notation

$$R_j = \sum_{i=0}^{j} (P_i + M_i), \tag{29}$$

with the convention $R_0 = 0$, and the result $N = R_K$. The FE and SE for the present case may be obtained by generalizing the procedure described in the previous section. Detailed derivations are, however, too lengthy to be reported. Let us only mention that, when writing the basic equations, we isolate

$$\varphi_{j+1} - \alpha_{j+1} = 2\omega_j + \varphi_j + \alpha_j, \quad j = R_{K-1} + M_K - 1, \tag{30}$$

which is to be used to establish the SE.

For the FE, we then obtain

$$-\cos(\varphi_0+\alpha_0)=\left\{\cos(\varphi_{M_1}-\alpha_{M_1})+\sum_{i=1}^{M_1-1}\left[\cos(\varphi_{R_0+i}+\alpha_{R_0+i})+\cos(\varphi_{R_0+i}-\alpha_{R_0+i})\right]\right\}_{P_1M_1}$$
$$+\left\{\cos(\varphi_{R_1}+\alpha_{R_1})+\cos(\varphi_{R_1+M_2}-\alpha_{R_1+M_2})+\sum_{i=1}^{M_2-1}\left[\cos(\varphi_{R_1+i}+\alpha_{R_1+i})+\cos(\varphi_{R_1+i}-\alpha_{R_1+i})\right]\right\}_{P_2M_2}$$
$$+\left\{\cos(\varphi_{R_2}+\alpha_{R_2})+\cos(\varphi_{R_2+M_3}-\alpha_{R_2+M_3})+\sum_{i=1}^{M_3-1}\left[\cos(\varphi_{R_2+i}+\alpha_{R_2+i})+\cos(\varphi_{R_2+i}-\alpha_{R_2+i})\right]\right\}_{P_3M_3}$$
$$+\cdots+\left\{\cos(\varphi_{R_{K-1}}+\alpha_{R_{K-1}})+\cos(\varphi_{R_{K-1}+M_K}-\alpha_{R_{K-1}+M_K})+\sum_{i=1}^{M_K-1}\left[\cos(\varphi_{R_{K-1}+i}+\alpha_{R_{K-1}+i})\right.\right.$$
$$\left.\left.+\cos(\varphi_{R_{K-1}+i}-\alpha_{R_{K-1}+i})\right]\right\}_{P_KM_K}, \tag{31}$$

in which each term of the form $\{\}_{p_jM_j}$ is specific of the partial sequence P_jM_j in the mapping sequence.

We also have, for the $\{\}_{P_1M_1}$ term

$$\varphi_j-\alpha_j=\varphi_{R_0+j}-\alpha_{R_0+j}=\varphi_0+\alpha_0+2\left[\sum_{i=0}^{j-1}\omega_i+\sum_{i=1}^{j-1}\alpha_i\right],$$
$$j=1\ldots M_1, \tag{32}$$

$$\varphi_j+\alpha_j=\varphi_0+\alpha_0+2\left[\sum_{i=0}^{j-1}\omega_i+\sum_{i=1}^{j}\alpha_i\right],\quad j=1\ldots M_1. \tag{33}$$

Note that, in Eq. (33), we only need j up to (M_1-1) for insertion in the $\{\}_{P_1M_1}$ term of Eq. (31). It is, however, a fact that Eq. (33) also holds for $j=M_1$. Similar remarks will also be valid in the sequel, but will not be repeated any more. Eqs. (32)–(33) are complemented by:

$$\omega_j=\arcsin\left\{\frac{1}{r}\left[-\sin\alpha_j-d\cos\left(\varphi_0+\alpha_0+2\sum_{i=0}^{j-1}\omega_i+2\sum_{i=1}^{j}\alpha_i\right)\right]\right\},\quad j=0\ldots M_1-1, \tag{34}$$

$$\alpha_j=\arcsin\left[-r\sin\omega_{j-1}+d\cos\left(\varphi_0+\alpha_0+2\sum_{i=0}^{j-1}\omega_i+2\sum_{i=1}^{j-1}\alpha_i\right)\right],\quad j=1\ldots M_1. \tag{35}$$

For the $\{\}_{P_2M_2}$ term, we use

$$\varphi_{R_1}+\alpha_{R_1}=(\varphi_{M_1}-\alpha_{M_1})+P_1\pi+2(P_1+1)\alpha_{M_1}, \tag{36}$$

with $(\varphi_{M_1}-\alpha_{M_1})$ and α_{M_1} available from Eqs. (32) and (35), respectively. We also have

$$\varphi_{R_1+i}-\alpha_{R_1+i}=(\varphi_{R_1}+\alpha_{R_1})+2\left[\sum_{j=0}^{i-1}\omega_{R_1+j}+\sum_{j=1}^{i-1}\alpha_{R_1+j}\right],$$
$$i=1\ldots M_2, \tag{37}$$

$$\varphi_{R_1+i}+\alpha_{R_1+i}=(\varphi_{R_1}+\alpha_{R_1})+2\left[\sum_{j=0}^{i-1}\omega_{R_1+j}+\sum_{j=1}^{i}\alpha_{R_1+j}\right],\quad i=1\ldots M_2, \tag{38}$$

$$\omega_{R_1}=\arcsin\left\{\frac{1}{r}\left[-\sin\alpha_{M_1}-d\cos(\varphi_{R_1}+\alpha_{R_1})\right]\right\}, \tag{39}$$

$$\alpha_{R_1+j}=\arcsin\left[-r\sin\omega_{R_1+j-1}+d\cos(\varphi_{R_1+j}-\alpha_{R_1+j})\right],$$
$$j=1\ldots M_2, \tag{40}$$

$$\omega_{R_1+j}=\arcsin\left\{\frac{1}{r}\left[-\sin\alpha_{R_1+j}-d\cos(\varphi_{R_1+j}+\alpha_{R_1+j})\right]\right\},\quad j=1\ldots M_2-1. \tag{41}$$

For higher-order $\{\}_{P_jM_j}$ terms, excepted for the last term $\{\}_{P_KM_K}$, which will receive a special treatment, we use

$$\varphi_{R_n}+\alpha_{R_n}=(\varphi_{R_{n-1}+M_n}-\alpha_{R_{n-1}+M_n})+P_n\pi+2(P_n+1)\alpha_{R_{n-1}+M_n},\quad n=1\ldots K-2, \tag{42}$$

$$\varphi_{R_n+i}-\alpha_{R_n+i}=(\varphi_{R_n}+\alpha_{R_n})+2\left[\sum_{j=0}^{i-1}\omega_{R_n+j}+\sum_{j=1}^{i-1}\alpha_{R_n+j}\right],\quad n=0\ldots R_{K-2},\quad i=1\ldots M_{n+1},\tag{43}$$

$$\varphi_{R_n+i}+\alpha_{R_n+i}=(\varphi_{R_n}+\alpha_{R_n})+2\left[\sum_{j=0}^{i-1}\omega_{R_n+j}+\sum_{j=1}^{i}\alpha_{R_n+j}\right],\quad n=0\ldots R_{K-2},\quad i=1\ldots M_{n+1},\tag{44}$$

$$\omega_{R_n}=\arcsin\left\{\frac{1}{r}[-\sin\alpha_{R_{n-1}+M_n}-d\cos(\varphi_{R_n}+\alpha_{R_n})]\right\},\tag{45}$$

$$\alpha_{R_n+j}=\arcsin[-r\sin\omega_{R_n+j-1}+d\cos(\varphi_{R_n+j}-\alpha_{R_n+j})],\quad j=1\ldots M_{n+1},\tag{46}$$

$$\omega_{R_n+j}=\arcsin\left\{\frac{1}{r}[-\sin\alpha_{R_n+j}-d\cos(\varphi_{R_n+j}+\alpha_{R_n+j})]\right\},\quad j=1\ldots M_{n+1}-1.\tag{47}$$

As previously mentioned, the last term $\{\}_{P_KM_K}$ requires a special treatment. This is due to the fact that Eq. (30) has been isolated to generate the SE. The choice, for this isolation, is due to the fact that Eq. (30) appears near the bottom of the list of basic equations. We then establish

$$\varphi_{R_{K-1}}+\alpha_{R_{K-1}}=(\varphi_{R_{K-2}+M_{K-1}}-\alpha_{R_{K-2}+M_{K-1}})+P_{K-1}\pi+2(P_{K-1}+1)\alpha_{R_{K-2}+M_{K-1}},\tag{48}$$

$$\varphi_{R_{K-1}+i}-\alpha_{R_{K-1}+i}=(\varphi_{R_{K-1}}+\alpha_{R_{K-1}})+2\left[\sum_{j=0}^{i-1}\omega_{R_{K-1}+j}+\sum_{j=1}^{i-1}\alpha_{R_{K-1}+j}\right],\quad i=1\ldots M_{K-1},\tag{49}$$

$$\varphi_{R_{K-1}+i}+\alpha_{R_{K-1}+i}=(\varphi_{R_{K-1}}+\alpha_{R_{K-1}})+2\left[\sum_{j=0}^{i-1}\omega_{R_{K-1}+j}+\sum_{j=1}^{i}\alpha_{R_{K-1}+j}\right],\quad i=1\ldots M_K-1,\tag{50}$$

$$\alpha_{R_{K-1}}=\alpha_{R_{K-2}+M_{K-1}},\tag{51}$$

$$\omega_{R_{K-1}}=\arcsin\left\{\frac{1}{r}[-\sin\alpha_{R_{K-2}+M_{K-1}}-d\cos(\varphi_{R_{K-1}}+\alpha_{R_{K-1}})]\right\},\tag{52}$$

$$\alpha_{R_{K-1}+j}=\arcsin[-r\sin\omega_{R_{K-1}+j-1}+d\cos(\varphi_{R_{K-1}+j}-\alpha_{R_{K-1}+j})],\tag{53}$$

$$\omega_{R_{K-1}+j}=\arcsin\left\{\frac{1}{r}[-\sin\alpha_{R_{K-1}+j}-d\cos(\varphi_{R_{K-1}+j}+\alpha_{R_{K-1}+j})]\right\},\quad j=1\ldots M_K-1,\tag{54}$$

$$\varphi_{R_{K-1}+M_K}-\alpha_{R_{K-1}+M_K}=\varphi_0-P_K\pi-(2P_K+1)\alpha_0.\tag{55}$$

Finally, starting from Eq. (30), we establish the SE reading as

$$2\omega_{R_{K-1}+M_K-1}+2\alpha_{R_{K-1}+M_K-1}+(\varphi_{R_{K-1}+M_K-1}-\alpha_{R_{K-1}+M_K-1})-\varphi_0+P_K\pi+(2P_K+1)\alpha_0=0,\tag{56}$$

in which all terms may be explicitly expressed versus φ_0 and α_0 by using previously established formulas and in which, as in some previous cases, the exact modulo determination to be used may need to be adjusted.

III. DETECTION, VALIDATION, AND CATALOG OF ADMISSIBLE REPRESENTATIVES

A. Detection and validation

Let us consider arbitrary initial conditions (φ_n,α_n) in the phase space and their Nth iterate $(\varphi_{n+N},\alpha_{n+N})$. Let us introduce

$$\Delta\alpha(N)=\alpha_{n+N}-\alpha_n,\tag{57a}$$

$$\Delta\varphi(N)=\varphi_{n+N}-\varphi_n,\quad \text{modulo } 2\pi.\tag{57b}$$

We also introduce a distance D defined as

$$D(N)=\Delta\varphi(N)^2+\Delta\alpha(N)^2.\tag{58}$$

Under these circumstances, according to Eq. (9), the initial conditions (φ_n,α_n) generate a periodic orbit of period N if and only if $D\ (N)=0$. We then developed a graphical software displaying $D\ (N)$, for N given, in a grayscale fashion, with darker zones corresponding to smaller values of D and with a $D_{\max}$ value defining the grayscale levels. Scanning over (φ_n,α_n), we then obtain grayscale charts, called distance charts displayed, for $N=1,\ldots,6$, with $D_{\max}=1$, in Fig. 4. There is a fast increase of the complexity of the charts when N increases.

FIG. 4. Distance chart for $N=6$, $D_{\max}=1$.

Visually, these charts exhibit a fairly good symmetry with respect to $\alpha=0$. This symmetry is the consequence of the time reversal symmetry associated with reversals of mapping sequences. The symmetry is, however, not perfect, because the distance charts in Fig. 4 are for $D_{\max}\neq 0$. For $D_{\max}=0$, the symmetry would be perfect (as it is in the Hamiltonian chart).

To detect candidates for periodic orbits, in a distance chart for period N, we, therefore, have to explore the grayscale landscape (a rather lengthy procedure when N is large). This exploration is carried out by a combination of zooms and decreases of nominal $D_{\max}$ distances down to altitude zero. Periodic orbits are then located at the bottom of wells. These wells may be much elongated as already apparent in the distance chart, for $N=1$, displaying two wells associated with two different inclusion-touching periodic orbits [and for ($N=1$) with two different equivalence classes, each equivalence class containing only one element].

Distance charts exhibit inclusion touching and non-inclusion-touching periodic orbits. As previously mentioned, we are only interested in inclusion-touching periodic orbits. However, there also exist grazing periodic orbits that may be simultaneously viewed as inclusion touching and as non-inclusion-touching periodic orbits. Referring to the hitting condition of relation (1), grazing periodic orbits exhibit M_1 mappings for which r in the left-hand side (lhs) is just equal to the quantity in the right-hand side (rhs). Accordingly, all inclusion-touching periodic orbits are found to be isolated (this means with isolated locations in the distance chart) excepted for grazing periodic orbits that are connected with non-inclusion-touching periodic orbits. Due to the rotational invariance of the circular billiard, non-inclusion-touching periodic orbits are not isolated. They appear on continuous lines (KAM curves). These lines, similarly as in Fig. 3, may be located at the top and bottom of the distance charts (large $|\alpha|$'s) and, for N large enough, would correspond to genuine morphology-dependent-resonances, i.e., to genuine whispering gallery modes. They also may be located at smaller values of $|\alpha|$, and then are not genuine MDRs, because they allow refractive escapes [like 2 (1) 2 in the catalog with the inclusion removed].

Then any inclusion-touching periodic orbit, including any grazing periodic orbit, is isolated with respect to any other inclusion-touching periodic orbit. Therefore, for each detected candidate, the exploration of the distance charts provides us with a couple (φ_n,α_n) of initial conditions generating the periodic orbit, by using successive zooms and $D_{\max}$ distance decreases. Note, however, that the couple (φ_n,α_n) is not necessarily the couple (φ_0,α_0) of an admissible representative of an equivalence class.

For any (φ,α), and a present N, the software allows one, in a secondary window, to visualize the associated piece of trajectory, in the physical space of the annular billiard. Therefore, any candidate generated by the initial conditions (φ_n,α_n) may be visualized too. However, this visual observation is not sufficient to validate the candidate because, in practice, numerical limitations prevent us from decreasing $D_{\max}$ down to altitude 0 (which is, therefore, never reached) and because the vizualisation is limited by pixel resolution. Therefore, once a candidate is detected, it has to be validated (in practice, we essentially limited ourselves to the validation of an admissible representative in the equivalence class). Validations are carried out by using the algebraic expressions of the basic equations (Sec. II G) or of the derived equations (Secs. II H and II I). These algebraic expressions may be investigated by using algebraic solving (by hand, or with the assistance of an algebraic solver from a symbolic computation software) or numerical solving. In the last case, we used a numerical solver having the two following properties: (i) in general, the solver only computes a single real root, (ii) the solver may fail to find a root even though there is one: in such a case, specifying appropriate range information may result in a successful computation.

Accounting for these specifications, the strategy for validation by using the numerical solver is as follows. Appropriate ranges are always used, either relying on measuring angles on a drawing of the candidate (this may be sufficient), or by using accurate locations measured on a distance chart. Successful computations, therefore, validate the candidate. Unsuccessful computations, conversely, are not sufficient for rejection which then, could only be reliably based on analytical arguments. However, in practice, ambiguous cases have not been met.

B. Catalog

The system under study exhibits temporal symmetries, namely, time translational invariances and time reversal invariance (equivalence of mapping sequences through shifts and reversal), leading to the definition of equivalence classes of periodic orbits. It also exhibits a spatial symmetry, namely, mirror symmetry with respect to the axis $0y$ (Fig. 1). As a result, there exist two kinds of periodic orbits (i) symmetrical periodic orbits that intrinsically exhibit the mirror symmetry and (ii) nonsymmetrical periodic orbits that must occur by pairs, the mirror symmetry then relating the two companions of the pair.

The catalog, given in Fig. 5, gathers symmetrical admissible representatives for N from 1 to 6 and nonsymmetrical admissible representatives (only one companion in a pair) for $N=1$ to 5 (with a single admissible representative for each equivalence class).

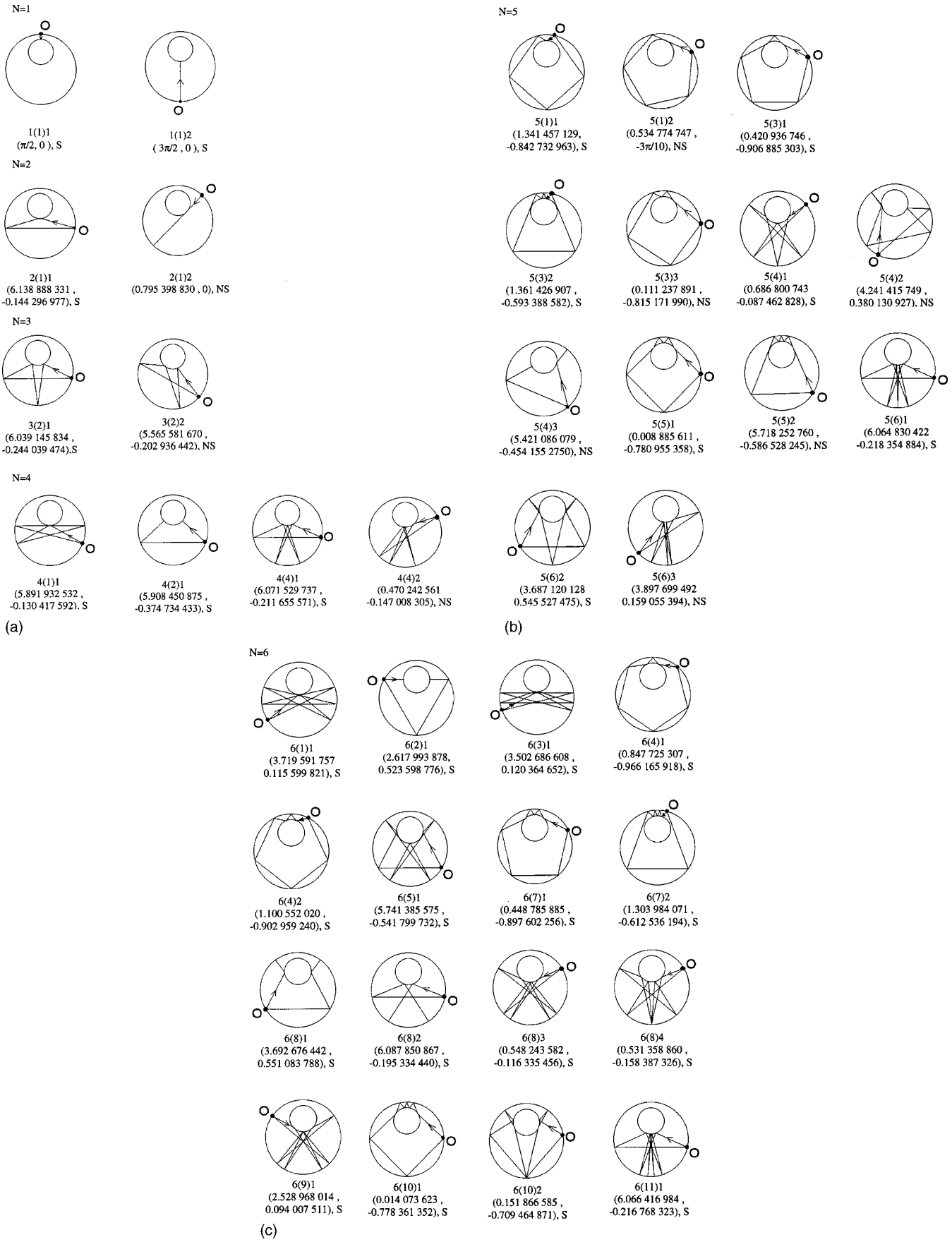

FIG. 5. Catalog of admissible representatives of periodic orbits.

Validations of all these representatives require a considerable amount of algebra and are sketched in the Appendix. Obviously, symmetrical representatives exhibit extrarelations, called symmetry relations. These relations allow one to simplify the algebra and, very often, it is possible to reduce the set of two equations for (φ_0,α_0) to a single equation for α_0. Examples of symmetry relations are Eqs. (A35)–(A40) for the orbit 5 (4) 1 (see, the Appendix). Extra simplifications may also occur when the orbit under study is degenerate, leading to extrarelations called degeneracy equations (Sec. III D).

The catalog contains one admissible representative for each detected and validated equivalence class, with a label 0 for the initial point (φ_0) and an arrow of time (sign of α_0), generating an admissible mapping sequence. Each representative receives a name having the expression A (B) C in which A (B) is the label of the mapping sequence (Table I) and C is an ordinal positive integer $(1, 2 \ldots)$ allowing one to distinguish different admissible representatives having the same admissible mapping sequence. For a given label A (B), the value of C for any symmetrical orbit in the catalog is smaller than for any nonsymmetrical orbit in the catalog. In particular, this ensures us that the names of the symmetrical periodic orbits of the catalog for $N=6$, would not be modified if this part of the catalog were extended to nonsymmetrical orbits. Afterward, we provide the values (φ_0,α_0) defining the initial point 0 and, finally, a label S (NS) indicates whether the orbit is symmetrical (nonsymmetrical).

C. Occurrences of equivalence classes

We observe that all admissible mapping sequences are actually not present in the catalog. Occurrences of admissible mapping sequences are displayed in the last column of Table I, in which, for each admissible mapping sequence, a label AS indicates A occurrences of symmetrical representatives in the catalog and a label ANS indicates A occurrences of nonsymmetrical pairs of representatives in the catalog.

For $N=6$, two admissible mapping sequences do not generate any representative in the catalog but recall that, for this value of the period, nonsymmetrical periodic orbits have not been cataloged. Lacking admissible representatives, and, therefore, lacking equivalence classes, also appear for $N=2 \ldots 5$. In some cases, lacking equivalence classes could possibly exist for other values of the control parameters (i.e., $d\neq 0,\ 5,\ r\neq 0,\ 35$) in connection with the thema of bifurcations of periodic orbits. In other cases, the lack of equivalence classes could be deeply structural, i.e., independent of the control parameters. This thema of occurrences of equivalence classes is not extensively investigated in this paper but we shall study, as an example, the case of the admissible mapping sequence 11.

A periodic orbit with mapping sequence 11 must start from a point A on the host circle, impinge on the inclusion at B, reaches the host circle at C (first M_1 mapping) and go back to A following the reverse path (second M_1 mapping). Therefore, the normal to the inclusion at B must be an axis of symmetry. Since $0y$ is the only axis of symmetry available, periodic orbits with mapping sequence 11 can be as sketched in Figs. 6(a) or 6(b) (opportunities). In both cases, we have the symmetry relations

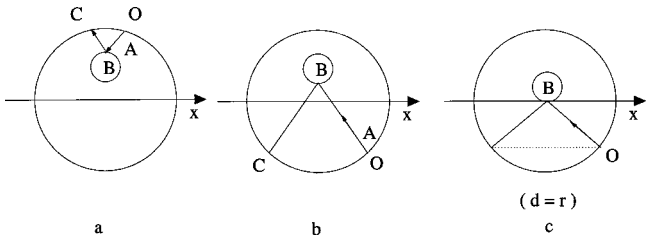

FIG. 6. Research of periodic orbits with mapping sequences 11. (a) and (b): opportunities (c) actual occurrences.

$$\alpha_1=\alpha_0=0, \tag{59}$$

$$\omega_1=-\omega_0, \tag{60}$$

and, depending on the case

$$(6a)\quad \varphi_1=\pi-\varphi_0, \tag{61}$$

$$(6b)\quad \varphi_1=3\pi-\varphi_0. \tag{62}$$

Then, we write the basic equations for the mapping sequence 11, and implement Eqs. (59) and (60). In case (6a), we obtain $r/d=-1$, which is impossible. In case (6b) we conversely obtain $r/d=1$. Therefore, the mapping sequence 11 is forbidden if $r\neq d$. If $r=d$, we obtain the picture sketched in Fig. 6(c) with a tangency between the inclusion and the axis $0x$. Simple geometrical considerations demonstrate that periodic orbits with sequence 11 indeed exist when $r=d$. Furthermore, in agreement with the solution $r=d$, we may geometrically check that the value of φ_0 does not matter as far as $\varphi_0\in[\pi,2\pi]$. For $\varphi_0=3\pi/2$, we recover period-one orbits previously described. Period-two orbits with sequence 11, therefore, generically do not occur, i.e., they only occur for $r=d$ and an infinitesimal perturbation from this solution makes them forbidden via what we may call an abrupt bifurcation.

In principle, such approaches should allow one to investigate lacking equivalence classes, i.e., equivalence classes that do not generate any actual representative, in order to determine how such a lacking property might depend on the control parameters.

In the same spirit, we may observe, for control parameters different than $d=0,\ 5$, $r=0,\ 35$, a periodic orbit having the same structure than our 6 (2) 1 in Ref. [13], and a periodic orbit having the same structure than our 6 (8) 1 in Ref. [14].

D. Degeneracy relations

We introduce several cases of degeneracy, starting with degeneracy with respect to phase space coordinates and afterward, ending with degeneracy with respect to control parameters.

A periodic orbit is α degenerate iff one or several α's in the sequence $(\alpha_0,\alpha_{1\ldots}\alpha_{N-1})$ is zero. In the catalog, the following representatives are α degenerate: 1 (1) 1, 1 (1) 2, 2 (1) 2, 5 (4) 3, 6 (8) 1, and 6 (8) 2. Each α degeneracy implies

a relation, i.e., $\alpha_i=0$ for some i, which is a degeneracy relation.

A periodic orbit is φ degenerate iff some φ's in the sequence $(\varphi_0,\varphi_1\ldots\varphi_{N-1})$ identify. In the catalog, the following representatives are φ degenerate: 4 (2) 1, 5 (4) 3, 6 (2) 1, 6 (8) 1, 6 (8) 2, 6 (8) 4, and 6 (10) 2. Each φ degeneracy implies a relation, i.e., $\varphi_i=\varphi_j$ for some i and some j, which is a degeneracy relation.

α degeneracy and φ degeneracy are two different kinds of degeneracy. This means that a periodic orbit can be α degenerate and not φ degenerate [for instance, 1 (1) 1] and that an orbit can be φ degenerate and not α degenerate [for instance, 4 (2) 1]. However, an orbit can be $\alpha\varphi$ degenerate [5 (4) 3, 6 (8) 1, 6 (8) 2].

A degeneracy relation can be a symmetry relation. In such a case, the degeneracy relation is a consequence of the symmetry of a symmetrical orbit. For instance, in 1 (1) 1, the α-degeneracy relation $\alpha_0=0$ is a symmetry relation. Also, in 6 (8) 4, the φ-degeneracy relation $\varphi_4=\varphi_1$ is a symmetry relation. Conversely, the nonsymmetrical representative 5 (4) 3, for instance, exhibits $\alpha\varphi$-degeneracy relations that are not symmetry relations. Degeneracy relations that are not symmetry relations provide extra relations that may lead to easier validations of the detected representatives.

Degeneracy may also be defined with respect to control parameters, and taken as the definition of structural stability of the periodic orbit under discussion. By definition, d degeneracy means that we may continuously change the value of d, without destroying the periodic orbit.

For instance, the orbits 1 (1) 1 and 1 (1) 2 are d degenerate. If $d=0$, we also possess two extra-period 1 orbits along axis $0x$. These orbits, however, are not d degenerate. Establishing a d-degeneracy usually requires specific investigations.

Furthermore, by definition, r degeneracy means that we may continuously change the value of r, without destroying the orbit. Also, establishing a r degeneracy usually requires specific investigations but, as a sufficient condition for r degeneracy, we have the nullity of all ω's. According to this sufficient criterion, here is a list of r degenerate orbits: 1 (1) 1 and 1 (1) 2 with $\omega_0=0$, 4 (2) 1 with $\omega_0=\omega_2=0$, and 6 (2) 1 with $\omega_0=\omega_3=0$.

E. Occurrences in phase space, and exhaustivity

Let us consider an equivalence class of period N with the representative in the catalog (and, therefore, all periodic orbits in the equivalence class) without any degeneracy with respect to phase space coordinates. This class must occur $2N$ times in the phase space and, more important, $2N$ times in the distance chart (N possible values for φ due to time shifts and two possibilities for α due to time reversal invariance).

We say that the occurrence is $2N$ in the $(\varphi,\ \alpha)$ plane. Degeneracy with respect to phase space coordinates decreases the number of occurrences in the $(\varphi,\ \alpha)$ plane. For instance, the equivalence class of 4 (2) 1 contains only $N=4$ elements (since there are only two distinct impacts on the host circle) instead of $2N=8$ and, similarly the equivalence class of 6 (2) 1 contains only $N=6$ elements, instead of $2N=12$. These elements are clearly exhibited in the Hamiltonian chart of Fig. 3 (we shall return to them later). Furthermore, the number of occurrences for a nonsymmetrical equivalence class may be thought as being twice larger than for a symmetrical equivalence class since the detection of a periodic orbit in a pair implies the existence of its companion, leading to $4N$ detection opportunities in a nondegenerate case.

Next, periodic orbits of period p in a p-distance chart also occur under the form of periodic orbits of period kp (k a positive integer) in a kp-distance chart. Finally, there is no universal strategy to explore a distance chart (depending for instance on the complexity of the chart) but zooms and subzooms are used. Therefore, a periodic orbit, for a distance D not too close to zero, may be detected on several subzooms when the wells surrounding the associated point of altitude zero are elongated enough.

Next, the methodology used to detect equivalence classes does not allow one to pretend to full exhaustivity. However, to miss an equivalence class, we have to miss all elements of the class. Since many opportunities are offered for the detection of an equivalence class as described above, the probability for exhaustivity is certainly very close to 1.

F. Grazing periodic orbits

In the annular billiard, first locate a periodic orbit of the circular billiard that (if possible) does not interact with the inclusion. Then, keeping the inclusion at rest, rotate the host circle and its attached periodic orbit until the orbit just touch the inclusion (if possible). This process, when it works, generates a grazing periodic orbit of the annular billiard.

The circular billiard does not possess any periodic orbit of period 1. Accordingly, there is no period-1 grazing periodic orbit (catalog of Fig. 5). For $N=2$, consider a periodic orbit of the circular billiard (a diametral chord), which does not touch the inclusion, for instance, aligned along the axis $0x$. Let us remark that this orbit impinges at right angles on the host circle ($\alpha_1=\alpha_0=0$) and, therefore, is not a MDR (due to refractive escape). A rotation then may generate the representative named 2 (1) 2.

For $N=3$, 4, and 6, we did not observe any grazing periodic orbit of the annular billiard. Invoking the rotational scenario described above, we should be able to determine whether such orbits are forbidden (for $d=0.5$, $r=0.35$) or whether they have been missed during the exploration of the distance charts.

For $N=5$, we have candidates based on pentagons inscribed in the circular billiard. Such pentagons may surround the inclusion and, upon rotation, become grazing. The proof is by displaying an example, namely, the representative 5 (1) 2 in the catalog.

The interest of a focus on grazing periodic orbits is, therefore, warranted (and postponed to a future work). Let us here remark that, for a given admissible mapping sequence $A(B)$, grazing periodic orbits in the catalog received the largest integer C in the names $A\ (B)\ C$. Therefore, grazing periodic orbits that would possibly be missed could be added in the catalog without any inconvenience.

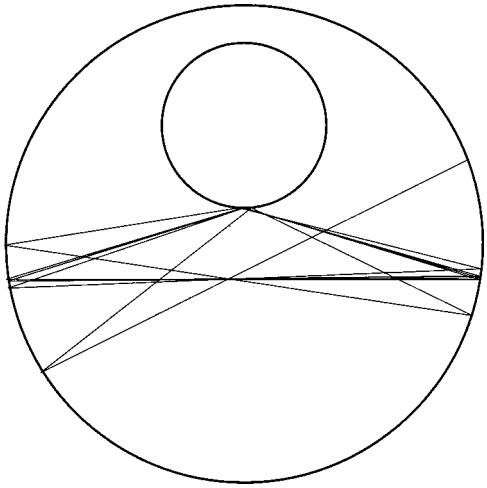

FIG. 7. Orbit 2 (1) 1 after 30 iterations (unstable).

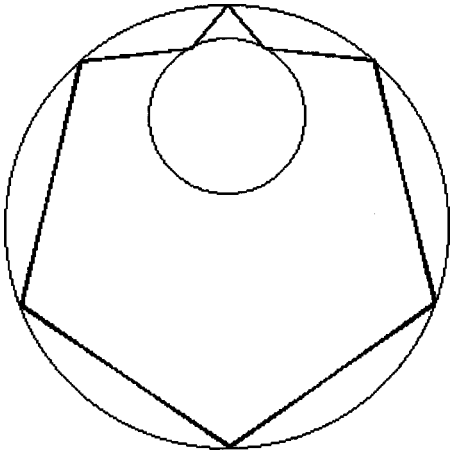

FIG. 8. Stable orbit 6 (4) 1 after 10^5 iterations. Initial conditions with three decimal digits.

G. Stability

Once a periodic orbit is determined, it is important to know whether this orbit is stable or not. Here, following Berry [5], a periodic orbit starting from original canonical (i.e., area preserving) variables (s, p) may be stable or unstable in the sense that an orbit starting at $(s+\delta s, p+\delta p)$, where δs and δp are small, may after many impacts (on the host circle) remain near the periodic orbit generated by (s, p) or may deviate increasingly from it. For a period-N orbit, after N iterations, s and p return to their initial values while the deviations of the nearby orbit starting from $(s+\delta p, p+\delta p)$ become $(\delta s_N, \delta p_N)$ with

$$\begin{pmatrix} \delta s_N \\ \delta p_N \end{pmatrix} = M_N \begin{pmatrix} \delta s \\ \delta p \end{pmatrix}, \tag{63}$$

with M_N being a 2×2 matrix. Let T be the trace of the matrix M_N. Then, the periodic orbit is stable (unstable) when $|T|<2$ ($|T|>2$) [4,5]. It is marginally stable for $|T|=2$. More generally, the stability (instability) of a periodic orbit implies the stability (instability) of the associated equivalence class.

Relying on this formulation, it can be demonstrated that the periodic orbits 1 (1) 1 and 1 (1) 2 are both unstable. Another way to proceed is to iterate a large enough number of times and to graphically examine the behavior of the orbit in the annular space (then avoiding lengthy and tedious algebraic evaluations). In this paper, we shall be content to use this more expedient method for periods $N>1$.

All orbits of the catalog (excepted grazing orbits) have then been tested, starting from the nominal values given in the catalog, with nine decimal digits. Since these nominal values are actually rounded off, they correspond to nearby orbits with small δs and δp.

For unstable orbits, instabilities are always apparent after a small number of iterations, say 30, as exemplified in Fig. 7 and, after 1000 iterations, the annular space is essentially blackened. Only three equivalence classes have been found to be stable, with admissible representatives 4 (2) 1, 6 (2) 1, and 6 (4) 1. In these cases, representatives are essentially visually unchanged even after 100 000 iterations. A slight broadening may be observed, after 100 000 iterations, when the initial conditions are taken with three decimal digits, with an example in Fig. 8.

The degenerate stable equivalence classes of the representatives 4 (2) 1 and 6 (2) 1, having four and six occurrences in the phase space, are well visible in the Hamiltonian chart of Fig. 3 where they generate islands (KAM curves surrounding the elliptic points of the stable orbits). The islands associated with 6 (4) 1 can be detected after a zoom around the orbit locations. These islands are immersed in the chaotic sea generated by the unstable orbits.

H. On resonances

MDRs in the circular billiard share two properties (i) they are in resonance, that means they are periodic orbits with a phase-matching condition and (ii) they do not escape refractively. A periodic orbit of the circular billiard is not necessarily a MDR (a resonance) since the second property is not always satisfied. For example, the periodic orbit 2 (1) 2 is not a MDR since the incidence angle on the host circle leads to refractive escape in an extended light scattering problem.

The presence of the inclusion destroys a set of MDRs of the circular billiard and, in turn, generates new periodic orbits that may be resonances. The investigation of this issue, of much importance for electromagnetic scattering problems, is postponed to a future work.

Intuitively, we also expect that stable periodic orbits are of particular significance in light scattering problems. The examination of this expectation is another opportunity for future work. In particular, it is intuitively expected that the stable orbits 4 (2) 1 and 6 (2) 1 would provide specific signatures in the scattering diagrams, while 6 (4) 1 would significantly contribute to the structure of the internal electromagnetic fields.

IV. CONCLUSION

Periodic orbits in the annular billiard have been studied for specific values $(d,r)=(0.5,0.35)$ of the control param-

eters. A catalog of periodic orbits has been built relying on a two-step process. In the first step, candidates for admissible representatives of equivalence classes of periodic orbits are detected by exploring distance charts in phase space coordinates. In a second step, these candidates are validated (or rejected) from the analysis of the admissible mappings generating them. Interesting issues (grazing periodic orbits, analytical studies of stability, bifurcations under a change of the control parameters, properties of resonances created by the inclusion) are briefly considered, with more systematic investigations postponed to future works.

Beside the intrinsic interest of this work in the field of Hamiltonian chaos (in mechanical language) or of optical chaos (in geometrical optics language), we have a strong motivation for the associated extended electromagnetic scattering problem.

It is expected that features exposed in this paper would form a skeleton for electromagnetic wave interaction. A significant issue is related to the existence of new MDRs in the case of a sphere with an eccentrically located spherical inclusion. More generally, an effort devoted to these issues might contribute to the understanding of light scattering by nonhomogeneous spherical particles, and to optical characterizations of such particles.

APPENDIX: VALIDATIONS OF ADMISSIBLE REPRESENTATIVES OF THE CATALOG

This appendix presents the validations of the detected admissible representatives of the catalog. This represents a considerable amount of algebraic work that cannot be exposed in detail, even in an appendix. Therefore, most often, we only provide concise indications. More details are provided for a chosen set for their illustrative virtue, particularly in the case $N=5$, which exhibits an intermediary level of difficulty. Let us remark that, for a given representative, there are usually several validation strategies available. We cannot pretend that a chosen validation is necessarily the most efficient (this would require the examination of all options and would unduly extend the algebraic burden).

1 (1) 1 and 1 (1) 2

Easy algebraic validation ''by hand,'' by using the M_1 mapping, with $(\varphi_1,\alpha_1)=(\varphi_0,\alpha_0)$.

2 (1) 1

We use derived equations for the type 01. An algebraic solver (symbolic computation software) can deal with this case.

2 (1) 2

This representative satisfies $\alpha_0=0$, $\omega_0=\pi/2$, making the FE for the type 01 becoming an identity. Then, return to basic equations which, with $\alpha_1=\alpha_0=0$, $\omega_0=\pi/2$, readily determine φ_0, ''by hand'' computations.

3 (2) 1

We use basic equations and implement symmetry relations (implying $\varphi_0=2\pi+\alpha_0$), leading to a single equation for α_0 which is numerically solved.

3 (2) 2

Derived equations for the type 011 are numerically solved.

4 (1) 1

We use basic equations, implement symmetry relations, show that $\varphi_0=4\pi+3\alpha_0$, and establish a single equation for α_0, which may be solved with an algebraic solver.

4 (2) 1

Beside symmetry relations, this orbit exhibits degeneracy relations (such as $\omega_2=\omega_0=0$), which simplify the basic equations, allowing one to proceed with ''by-hand'' algebraic computations.

4 (4) 1

Using derived equations for the type 0111, using symmetry relations, and by invoking the M_0 map involved in the mapping sequence, we show that $\varphi_0=2\pi+\alpha_0$. We then obtain, from the FE, a single relation to determine α_0, which is numerically solved.

4 (4) 2

We use derived equations for the type 0111, and solve numerically.

5 (1) 1

We use derived equations for the sequence 00001, and write down the FE and the SE. Then, we write down the basic equations for the M_0 maps involved in the mapping sequence, being careful with the exact modulo determinations to be used, and show, with the aid of the symmetry relation $\varphi_1=(\pi-\varphi_0)$ that

$$\varphi_0=4\alpha_0+\frac{3\pi}{2}. \tag{A1}$$

We then observe that Eq. (A1) makes the FE being an identity. We establish that the SE may be written as

$$\sin(\omega_0+5\alpha_0)=0, \tag{A2}$$

with

$$\omega_0=\arcsin\left\{\frac{1}{r}[-\sin\alpha_0-d\sin(5\alpha_0)]\right\}, \tag{A3}$$

and use a numerical solver.

5 (1) 2

This orbit is a grazing orbit that is obtained by drawing a pentagon in the host circular billiard, and rotating it until it

just touches the inclusion. This geometrical observation allows us to use a particular procedure to validate the orbit. We write down the basic equations for the M_1 map involved in the sequence. Next, we have a grazing condition

$$\omega_0=\frac{\pi}{2}, \tag{A4}$$

and two relations characterizing the geometry of the pentagon

$$\varphi_1=\varphi_0+\frac{2\pi}{5}, \tag{A5}$$

$$\alpha_1=\alpha_0. \tag{A6}$$

Inserting Eqs. (A4)–(A6) in the previous basic equations, we readily obtain

$$\alpha_0=-\frac{3\pi}{10}, \tag{A7}$$

and

$$r=-\sin\alpha_0-d\cos(\varphi_0+\alpha_0), \tag{A8}$$

which, after insertion of Eq. (A7), may be solved with an algebraic solver.

5 (3) 1 and 5 (3) 2

We use the same procedure for both. We write the derived equations for the sequence 00011.

$$\cos(\varphi_0+\alpha_0)-\cos(\varphi_0-7\alpha_0)+\cos(\varphi_0+\alpha_0+2\omega_0+2\alpha_1)+\cos(\varphi_0+\alpha_0+2\omega_0)=0, \tag{A9}$$

$$\omega_0=\arcsin\left\{\frac{1}{r}[-\sin\alpha_0-d\cos(\varphi_0+\alpha_0)]\right\}, \tag{A10}$$

$$\alpha_1=\arcsin[-r\sin\omega_0+d\cos(\varphi_0+\alpha_0+2\omega_0)], \tag{A11}$$

$$4\alpha_0+\alpha_1+\omega_0+\omega_1=-\frac{3\pi}{2}, \tag{A12}$$

$$\omega_1=\arcsin\left\{\frac{1}{r}[-\sin\alpha_0-d\cos(\varphi_0-7\alpha_0)]\right\}. \tag{A13}$$

We have the symmetry relations

$$\omega_1=\omega_0, \tag{A14}$$

$$\varphi_2=\pi-\varphi_0, \tag{A15}$$

$$\alpha_2=\alpha_0. \tag{A16}$$

We write down the basic equations for the M_0 maps (with the exact modulo determination) and establish

$$\varphi_0=3\alpha_0+\pi. \tag{A17}$$

Equations (A9)–(A13) then reduce to a single equation for α_0,

$$\cos(4\alpha_0+2\omega_0)+\cos(4\alpha_0+2\omega_0+2\alpha_1)=0, \tag{A18}$$

$$\omega_0=\arcsin\left\{\frac{1}{r}[-\sin\alpha_0+d\cos(4\alpha_0)]\right\}, \tag{A19}$$

$$\alpha_1=\arcsin[-r\sin\omega_0-d\cos(4\alpha_0+2\omega_0)], \tag{A20}$$

which is numerically solved. The different orbits 5 (3) 1 and 5 (3) 2 are then validated by using different appropriate ranges for the numerical solver.

5 (3) 3

We numerically solve the derived equations (A9)–(A13) for the sequence 00011 (no symmetry). The checking of exact modulo determinations shows that Eq. (A12) is changed to

$$4\alpha_0+\alpha_1+\omega_0+\omega_1=-\frac{\pi}{2}. \tag{A21}$$

5 (4) 1

We use the derived equations for the sequence 01011. The FE reads as

$$-\cos(\varphi_0+\alpha_0)=\cos(\varphi_1-\alpha_1)+\cos(\varphi_1+\alpha_1)+\cos(\varphi_2-\alpha_2)+\cos(\varphi_3+\alpha_3)+\cos(\varphi_4-\alpha_4), \tag{A22}$$

$$(\varphi_1-\alpha_1)=\varphi_0+\alpha_0+2\omega_0, \tag{A23}$$

$$(\varphi_1+\alpha_1)=\varphi_0+\alpha_0+2\omega_0+2\alpha_1, \tag{A24}$$

$$(\varphi_2-\alpha_2)=\varphi_0+\alpha_0+2\omega_0+2\omega_1+2\alpha_1, \tag{A25}$$

$$\omega_0=\arcsin\left\{\frac{1}{r}[-\sin\alpha_0-d\cos(\varphi_0+\alpha_0)]\right\}, \tag{A26}$$

$$\alpha_1=\arcsin[-r\sin\omega_0+d\cos(\varphi_0+\alpha_0+2\omega_0)], \tag{A27}$$

$$\omega_1=\arcsin\left\{\frac{1}{r}[-\sin\alpha_1-d\cos(\varphi_0+\alpha_0+2\omega_0+2\alpha_1)]\right\}, \tag{A28}$$

$$\alpha_2=\arcsin[-r\sin\omega_1+d\cos(\varphi_0+\alpha_0+2\omega_0+2\omega_1+2\alpha_1)], \tag{A29}$$

$$(\varphi_3+\alpha_3)=(\varphi_2-\alpha_2)+4\alpha_2+\pi, \tag{A30}$$

$$(\varphi_4-\alpha_4)=\varphi_0-3\alpha_0-\pi. \tag{A31}$$

The SE reads as

$$\varphi_0-3\alpha_0-2\omega_3-2\alpha_2-(\varphi_3-\alpha_3)=\pi, \tag{A32}$$

$$\omega_3 = \arcsin\left\{\frac{1}{r}[-\sin\alpha_2 - d\cos(\varphi_3+\alpha_3)]\right\}, \quad \text{(A33)}$$

$$(\varphi_3-\alpha_3) = (\varphi_2-\alpha_2) + 2\alpha_2 + \pi. \quad \text{(A34)}$$

The set may be solved with a numerical solver. If we implement the symmetry relations

$$\varphi_2 = \pi - \varphi_0, \quad \text{(A35)}$$

$$\varphi_4 = 3\pi - \varphi_3, \quad \text{(A36)}$$

$$\varphi_1 = \frac{3\pi}{2}, \quad \text{(A37)}$$

$$\alpha_2 = \alpha_0, \quad \text{(A38)}$$

$$\alpha_4 = \alpha_3, \quad \text{(A39)}$$

$$\omega_1 = \omega_0, \quad \text{(A40)}$$

then the FE becomes an identity. Under such circumstances, we may return to the basic equations, implement the symmetry relations, and establish

$$\sin\alpha_0 + d\cos(\varphi_0+\alpha_0) = (1+d)\sin\alpha_1, \quad \text{(A41)}$$

$$\alpha_1 = \frac{3\pi}{2} - \varphi_0 - \alpha_0 - 2\omega_0, \quad \text{(A42)}$$

$$\omega_0 = \arcsin\left\{\frac{1}{r}[-\sin\alpha_0 - d\cos(\varphi_0+\alpha_0)]\right\}, \quad \text{(A43)}$$

$$3\alpha_0 - \varphi_0 + \omega_3 = -\frac{\pi}{2}, \quad \text{(A44)}$$

$$\omega_3 = \arcsin\left\{\frac{1}{r}[-\sin\alpha_0 - d\cos(\varphi_3+\alpha_0)]\right\}, \quad \text{(A45)}$$

$$\varphi_3 = 2\alpha_0 - \varphi_0 + 2\pi, \quad \text{(A46)}$$

in which Eq. (A41) is a FE and Eq. (A44) is a SE. The set may be solved with a numerical solver.

This example shows that there is generally not a unique validation strategy. The first approach avoids extra-algebraic manipulations required in the second approach but is numerically about 100 times slower.

5 (4) 2

We use the same derived equations than for the orbit 5 (4) 1, with a $(-\pi)$ modulo determination in the rhs of Eq. (A32), instead of a $(+\pi)$ determination, and solve numerically.

5 (4) 3

For this highly degenerate case, the SE becomes an identity. Therefore, we return to basic equations, implement degeneracy relations, obtain two new derived equations, and solve numerically.

5 (5) 1

We use the derived equations for the sequence 00111, implement the symmetry relations and, by using the last M_0 map in the mapping sequence, establish that $\varphi_0 = 2\alpha_0 + \pi/2$, leading to a single equation for α_0,

$$\sin(3\alpha_0+2\omega_0) + \sin(3\alpha_0+2\omega_0+2\alpha_1) + \sin(3\alpha_0+2\omega_0 + 2\omega_1+2\alpha_1) + \sin(3\alpha_0+2\omega_0+2\omega_1+4\alpha_1) = 0, \quad \text{(A47)}$$

$$\omega_0 = \arcsin\left\{\frac{1}{r}[-\sin\alpha_0 + d\sin(3\alpha_0)]\right\}, \quad \text{(A48)}$$

$$\alpha_1 = \arcsin[-r\sin\omega_0 - d\sin(3\alpha_0+2\omega_0)], \quad \text{(A49)}$$

$$\omega_1 = \arcsin\left\{\frac{1}{r}[-\sin\alpha_1 + d\sin(3\alpha_0+2\omega_0+2\alpha_1)]\right\}. \quad \text{(A50)}$$

5 (5) 2

We use the derived equations for the sequence 00111 (same as in the previous case), and solve numerically. However, let us remark that, in the previous case, the SE reads as

$$3\alpha_0 + \alpha_1 + \alpha_2 + \omega_0 + \omega_1 + \omega_2 = -\pi, \quad \text{(A51)}$$

while, in the present case, it reads as

$$3\alpha_0 + \alpha_1 + \alpha_2 + \omega_0 + \omega_1 + \omega_2 = 0, \quad \text{(A52)}$$

emphasizing once more that exact modulo determinations may have to be checked. The most expedient way is to check on the drawing of the candidate under study.

5 (6) 1

For this case, we use the derived equations for the sequence 01111 and solve them numerically. Another possibility is to also use the symmetry relations, invoke the M_0 mapping involved in the sequence to express $\varphi_0(\alpha_0)$ and generate a single equation for α_0.

5 (6) 2

Same as for 5 (6) 1.

5 (6) 3

We use the derived equations for the sequence 01111, and solve them numerically.

6 (1) 1

The derived equations for the sequence 000001 read as

$$\cos(\varphi_0+\alpha_0) - \cos(\varphi_0 - 11\alpha_0) = 0, \quad \text{(A53)}$$

$$\omega_0 + 6\alpha_0 = +\frac{\pi}{2}, \quad \text{(A54)}$$

$$r\sin\omega_0 = -\sin\alpha_0 - d\cos(\varphi_0+\alpha_0). \quad \text{(A55)}$$

This example is interesting for two reasons (i) it exemplifies once more that we have to be careful with modulo determinations since the rhs of Eq. (A54) must be $(+\pi/2)$ instead of $(-5\pi/2)$, as would be obtained from a naive interpretation of the derived equations and (ii) symmetry relations have not to be used to obtain simple enough equations.

Equations (A53)–(A55) are better rewritten as

$$\cos(\varphi_0+\alpha_0)-\cos(\varphi_0-11\alpha_0)=0, \tag{A56}$$

$$r\cos(6\alpha_0)=-\sin\alpha_0-d\cos(\varphi_0+\alpha_0), \tag{A57}$$

which are solved numerically.

6 (2) 1

Due to symmetry relations, and the high level of degeneracy, this orbit is easy to validate, whatever the method used.

6 (3) 1

We use the derived equations specified for the sequence 000101, being careful with the exact modulo determination for the SE, and solve numerically. The use of symmetry relations is not useful.

6 (4) 1 and 6 (4) 2

We use the derived equations for the sequence 000011 with correct modulo determinations for the SE, and the symmetry relation $\omega_1=\omega_0$, and solve numerically.

6 (5) 1

The FE with symmetry relations reduces to an identity. Returning to basic equations, we implement symmetry relations leading to $\varphi_0=2\pi+\alpha_0$, and derive a single equation for α_0, to be solved numerically.

6 (7) 1 and 6 (7) 2

We use the derived equations for the sequence 000111, with correct modulo determination for the SE, implement symmetry relations to obtain simplified FE and SE, and solve numerically.

6 (8) 1

With symmetry and degeneracy relations, the SE becomes an identity. Basic equations, however, lead to $\varphi_0=\pi+\alpha_0$, and to a single equation for α_0, to be solved numerically.

6 (8) 2

Same as for 6 (8) 1, but with $\varphi_0=2\pi+\alpha_0$.

6 (8) 3

With symmetry relations, the FE becomes an identity. Returning to basic equations and implementing symmetry relations, we may deduce new derived equations

$$2\sin\alpha_0+d[\cos(\varphi_0+\alpha_0)+\cos(\varphi_0-3\alpha_0)+\cos(\varphi_0+\alpha_0+2\omega_0)+\cos(\varphi_0-3\alpha_0+2\omega_1)]=0, \tag{A58}$$

$$\omega_0=-\arcsin\left\{\frac{1}{r}[\sin\alpha_0+d\cos(\varphi_0+\alpha_0)]\right\}, \tag{A59}$$

$$\omega_1=\arcsin\left\{\frac{1}{r}[\sin\alpha_0+d\cos(\varphi_0-3\alpha_0)]\right\}, \tag{A60}$$

$$r\sin\omega_0-\sin(\varphi_0-\alpha_0+\omega_0+\omega_1)-d\cos(\varphi_0+\alpha_0+2\omega_0)=0, \tag{A61}$$

which are solved numerically.

6 (8) 4

Same as for 6 (8) 3, with new derived equations reading as

$$\sin\alpha_0+d\cos(\varphi_0+\alpha_0)+(1+d)\cos(\varphi_0+\alpha_0+2\omega_0)=0, \tag{A62}$$

$$\sin\alpha_0+d\cos(\varphi_0-3\alpha_0)+(1+d)\cos(\varphi_0-3\alpha_0-2\omega_3)=0, \tag{A63}$$

$$\omega_0=-\arcsin\left\{\frac{1}{r}[\sin\alpha_0+d\cos(\varphi_0+\alpha_0)]\right\}, \tag{A64}$$

$$\omega_3=-\arcsin\left\{\frac{1}{r}[\sin\alpha_0+d\cos(\varphi_0-3\alpha_0)]\right\}. \tag{A65}$$

6 (9) 1

Same as 6 (8) 3 with the new derived equations reading as

$$\sin\alpha_0+d[\cos(\varphi_0+\alpha_0)+\cos(\varphi_0+\alpha_0+2\omega_0)]+(r-d)\sin\omega_1=0, \tag{A66}$$

$$\sin\alpha_0+(d-r)\cos(\varphi_0-3\alpha_0)=0, \tag{A67}$$

$$\omega_0=-\arcsin\left\{\frac{1}{r}[\sin\alpha_0+d\cos(\varphi_0+\alpha_0)]\right\}, \tag{A68}$$

$$\alpha_1=-\arcsin[r\sin\omega_0-d\cos(\varphi_0+\alpha_0+2\omega_0)], \tag{A69}$$

$$\omega_1=-\arcsin\left\{\frac{1}{r}[\sin\alpha_1+d\cos(\varphi_0+\alpha_0+2\omega_0+2d_1)]\right\}. \tag{A70}$$

6 (10) 1

We use derived equations for the sequence 001111, implement symmetry relations, check the exact modulo determination in the SE, and solve numerically.

6 (10) 2

We use derived equations for the sequence 001111, implement symmetry relations, invoke the last M_0 mapping to show that $\varphi_0 = 2\alpha_0 + \pi_2$, and establish a single relation for α_0, possibly to be solved numerically. This periodic orbit is actually particularly difficult to validate. The most expedient way has been to determine α_0 by trials and errors with a symbolic computation software.

6 (11) 1

We use derived equations for the sequence 011111, implement symmetry relations, invoke the M_0-mapping to show that $\varphi_0 = 2\pi + \alpha_0$, and establish a single relation for α_0, possibly to be solved numerically. Actually, as for the previous case, we solved the equation by trials and errors, with a symbolic computation software.

[1] *Optical Effects Associated With Small Particles*, edited by P. W. Barber and R. K. Chang (World Scientific, Singapore, 1998).

[2] S. C. Hill and R. E. Benner, in *Optical Effects Associated with Small Particles* (Ref. [1]), pp. 3–61.

[3] *Optical Processes in Microcavities*, edited by R. K. Chang and A. J. Campillo, Advanced Series in Applied Physics, Vol. 3 (World Scientific, Singapore, 1996).

[4] A. J. Lichtenberg and M. A. Lieberman, *Regular and Stochastic Motion*, Applied Mathematical Sciences, Vol. 38 (Springer-Verlag, Berlin, 1983).

[5] M. V. Berry, Eur. J. Phys. **2**, 91 (1981).

[6] V. Lefevre-Seguin, J. Knight, V. Sandoghar, D. S. Weiss, J. Hare, J. M. Raimond, and S. Haroche, in *Optical Processes in Microcavities* (Ref. [3]), pp. 101–133.

[7] H. B. Lin and A. J. Campillo, Opt. Lett. **20**, 1589 (1995).

[8] G. Gouesbet and G. Gréhan, Atomization Sprays **10**, 277 (2000).

[9] G. Gouesbet, L. Mees, and G. Gréhan, in Proceedings of the Tenth International Symposium on Applications of Laser Techniques to Fluid Mechanics, Lisbon, 2000 (unpublished). Paper available from the conference web site. To be republished in a conference selection book.

[10] K. F. Ren, G. Gréhan, and G. Gouesbet, Opt. Commun. **108**, 343 (1994).

[11] G. Gouesbet, Part. Part. Syst. Charact. **11**, 22 (1994).

[12] G. Gouesbet and G. Gréhan, J. Mod. Opt. **47**, 821 (2000).

[13] N. Saitô, H. Hirooka, J. Ford, F. Vivaldi, and G. M. Walker, Physica D **5**, 273 (1982).

[14] O. Bohigas, D. Boosé, R. Egydio de Carvalho, and V. Marvulle, Nucl. Phys. A **560**, 197 (1993).

[15] E. Doron and S. D. Frischat, Phys. Rev. Lett. **75**, 3661 (1995).

[16] G. Hackenbroich and J. U. Nöckel, Europhys. Lett. **39**, 371 (1997).

[17] J. U. Nöckel and A. D. Stone, in *Optical Processes in Microcavities* (Ref. [3]), pp. 389–426.

[18] A. D. Stone and J. U. Nöckel, Opt. Photonics News December, 37 (1997).

[19] J. U. Nöckel, A. D. Stone, and R. K. Chang, Opt. Lett. **19**, 1693 (1994).

[20] A. Mekis, J. U. Nöckel, G. Chen, A. D. Stone, and R. K. Chang, Phys. Rev. Lett. **75**, 2682 (1995).

[21] C. Letellier, G. Gouesbet, and N. F. Rulkov, Int. J. Bifurcation Chaos Appl. Sci. Eng. **6**, 2531 (1996).

[22] G. Boulant, M. Lefranc, S. Bielawski, and D. Derozier, Phys. Rev. E **55**, 5082 (1997).

[23] R. Gilmore, Rev. Mod. Phys. **70**, 1455 (1998).